Complexities of Transform Fault Plate Boundaries in the Oceans

Jeffrey J. McGuire

Woods Hole Oceanographic Institution, Woods Hole, Massachusetts

Thomas H. Jordan

University of Southern California, Los Angeles, California

Jian Lin

Woods Hole Oceanographic Institution, Woods Hole, Massachusetts

Deformation of oceanic plates is primarily confined to their boundaries, but some oceanic transform faults show geologic evidence for migration of the boundary across a wider zone. We test the extent to which the current deformation is localized into a single narrow fault valley for two such boundaries, the Romanche and Discovery II transform faults. Earthquake relocation reveals that some large earthquakes involve subevents, or even entire ruptures, that break sub-parallel faults offset from the primary plate boundary. This observation is confirmed through the estimation of the space-time rupture properties of the 1994 Romanche and 1997 Prince Edward Island earthquakes. Both events show strong directivity signals that are oriented at a high angle to both nodal planes of their moment-tensor and the strike of their respective main transform faults. These events began with episodes of smooth moment-release that radiated little high-frequency energy. The geometry of these events is consistent with the off-fault subevents being triggered by either the dynamic or static stress changes resulting from the slow components. Thus, these two plate boundaries show evidence for the interaction of multiple sub-parallel faults, suggesting that deformation beyond a single transform valley occurs on both geologic and coseismic time-scales.

1. INTRODUCTION

Transform fault boundaries between oceanic plates are generally very sharp features where all of the relative motion occurs across a narrow zone. This localization of deformation contrasts with transform fault boundaries occurring in continental regions, such as the western United States, where deformation can be accommodated by multiple geologic structures distributed over a

Plate Boundary Zones
Geodynamics Series 30

10/1029/030GD13

wide region. The region of oceanic crust affected by a transform fault, the transform domain [Fox and Gallo, 1984], can be several tens of kilometers wide and is usually centered on the transform valley. Within the transform domain, traces of active faulting are confined to a narrow region less than a few kilometers wide termed the principal transform displacement zone (PTDZ). The remainder of the transform valley, including the walls, generally lacks signs of recent activity. The PTDZ is considered to be the location of the current plate boundary within which all relative motion occurs. This localization of plate-motion within a belt $\leq$2 km wide appears to be enhanced for large offset transforms due to the thick lithosphere on the older side of the boundary [*Fox and Gallo*, 1984]. While the majority of present-day plate-motion is thought to be contained within the PTDZ, it is clear that on geologic time-scales deformation occurs over the broader region of the transform domain. This broader deformation is the result of migration of the principle transform fault within the fault valley as a response to changes in plate motion as well as non-transform deformation, such as the creation of transverse ridges. Occasionally the stresses resulting from changes in plate-motion are sufficiently large to cause the location of the boundary to jump to a new location outside the original transform valley [*Tucholke and Schouten,* 1988]. In such cases, the deformation appears to occur over a wide region on geologic time scales despite being localized at any one time. Even in steady-state geometries, plate motion can be partially accommodated by distributed deformation up to 20 km beyond the edge of the fault-valley resulting in measurable curvature of abyssal hill structures [*Fox and Gallo* 1994; *Sonder and Pockalny,* 1992].

There have been suggestions of active seismicity outside the PTDZ. An ocean bottom seismometer (OBS) study of microseismicity at the Kane transform recorded a significant number of events located outside the main transform valley [*Wilcock et al.,* 1990]. The subevent locations of large earthquakes determined by *McGuire et al.*[1996] and *McGuire and Jordan* [2000] from high-frequency travel-time picks suggest that present-day coseismic deformation may occur across a wide region at both the Romanche and Discovery II transforms.

2. GEOLOGIC OBSERVATIONS OF THE ROMANCHE TRANSFORM

The Romanche transform in the equatorial Atlantic is one of the most well documented examples of distributed deformation occurring in oceanic lithosphere on geologic time scales. At least four sub-parallel fault-valleys spanning a region 100-150 km wide are visible in gravity (Plate 1) and bathymetric [*Searle et al.,* 1994] maps of the western portion of the transform. The valley labeled C in Plate 1 has little to no sediment cover and contains the active transform fault that stretches for about 840 km between spreading segments. Valley D contains a paleotransform fault covered by 400-700m of sediment that can be traced from about 20° 20'W to 24° 20' W [*Searle et al.,* 1994]. The eastern limit of this valley indicates that it ceased being the primary transform fault at about 27 Ma [*Searle et al.,* 1994]. Valley B cuts through the northern transverse ridge to merge into the active transform valley near the eastern ridge-transform-intersection (RTI). It is covered in a few hundred meters of sediment and may have been the active trace of the Romanche transform before a change in plate motion occurred around 8-10 Ma [*Bonatti et al.,* 1994]. Valley A located just north of the northern transverse ridge is visible in the bathymetric map of *Searle et al.* [1994] and may also be a paleotransform valley. This suite of fault-valleys combined with evidence for a ridge-jump event about 5 Ma near the eastern RTI [*Bonatti et al.,* 1994] provides clear evidence that the exact location of this plate boundary changes regularly over geologic time. *Bonatti et al.* [2001] suggest that transform boundaries with age offsets greater than 30 Ma, such as Romanche and Andrew Bain, systematically prefer a multi-fault system as a response to the increased mechanical strength of their older lithosphere.

Perhaps the most spectacular evidence for the complex evolution of the Romanche transform boundary comes from the presence of a 140 Myr old limestone unit in the transverse ridge only about 100 km from the eastern RTI [*Bonatti et al.,* 1996] . To explain the presence of this unit and other continental material [*Bonatti* 1990] near the spreading axis of the MAR, *Bonatti et al.* [1994,1996] have proposed the oscillatory spreading hypothesis. In this model, the pieces of continental material have been repeatedly transferred back and forth between the African and South American plates owing to changes in the location of the transform and accretionary plate-boundaries. The most-recent episode of transform-fault migration appears to have transferred the material between valleys B and C in Plate 1 from the South American Plate to the African Plate at about 8-10 Ma [*Bonatti et al.,* 1994]. Thus, the location of the plate boundary may have shifted back and forth among the various faults shown in Figure 1 over geologic time in such a way that the Cretaceous limestone unit remained near the MAR for more than 100 Ma.

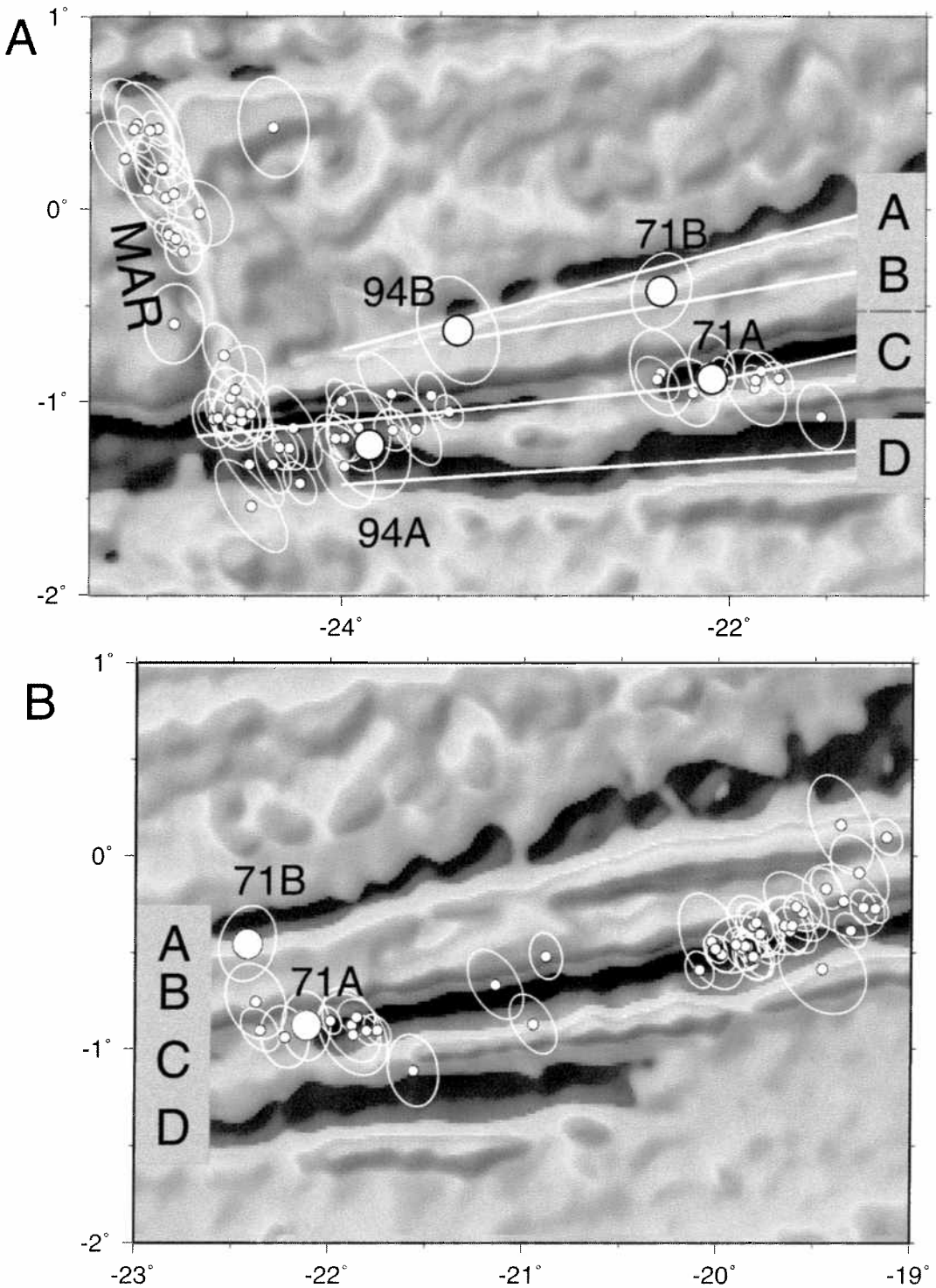

Plate 1. Maps showing the western portion of the Romanche transform. Colors are the satellite altimetric free-air gravity field [Sandwell and Smith, 1997]. The gravity anomalies range from -15 mGal (blue) to +15 mGal(red), and the relief is illuminated from the northwest. The four fault-valleys labeled A, B, C, and D are described in the text. MAR denotes the Mid-Atlantic Ridge. Small circles give locations and 95% confidence ellipses of the relocated background seismicity. Large circles denote locations and 95% confidence ellipses of the subevents of the 1971 and 1994 M_w 7.0 earthquakes.

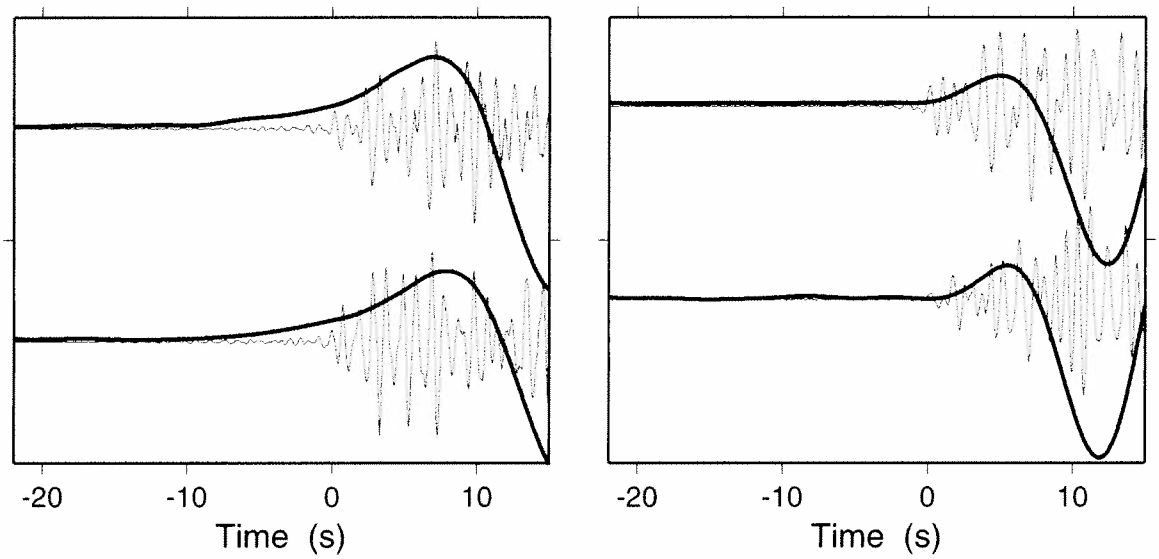

Figure 1. P wave seismograms for the 1997 Prince Edwards (left panel) and 1994 Northridge (right panel) events. Stations SA25 (top) and SA38 (bottom) from a temporary PASCAL array in soutern Africa are shown for the Prince Edwards Event, and stations CCM (top) and COL (bottom) are shown for the 1994 Northridge event. The thick traces are records that have been low-pass filtered with a causal 4-pole butterworth filter with a corner at .070 Hz, the thin traces have been high-pass filtered with a corner at 1 Hz.

3. SLOW EARTHQUAKES ON OCEANIC TRANSFORM FAULTS

Seismic activity on oceanic transform faults includes events with anomalously long durations that are termed "slow earthquakes" [*Kanamori and Stewart* 1976; *Okal and Stewart*, 1982]. *Okal and Stewart* [1982] noted that some oceanic transform events have large decreases in apparent size as a function of the frequency of the waves used to determine a particular magnitude scale. In particular, they found that m_b values (determined at 1 s), were often a full unit smaller than M_s (determined at 20 s) or M_w (determined at $\geq$ 100 s). *Okal and Stewart* [1982] also noted that events with $M_s - m_b \geq .9$ were associated with complex long-duration source-time functions. More recently the low values of m_b vs M_w for oceanic transform fault events have been verified by *Stein and Pelayo* [1991] and *Ihmle and Jordan* [1994] . *Kaverina et al.* [1996] suggested that the $M_s - m_b$ discrepancy observed on transform faults may be a global feature of faulting involving young oceanic lithosphere, including some subduction zones. *Stein and Pelayo* [1991] also compared computed source time function (STF) durations to seismic moments for a global catalog of oceanic earthquakes and found that oceanic transform fault events had anomalously long durations for their seismic moments relative to ridge and oceanic intraplate earthquakes. *Ihmle and Jordan* [1994] calculated a second-moment measure of the duration of earthquake STFs based on low-frequency amplitude spectra and found that many oceanic transform fault events have such anomalously long durations that they require a significant amount of low-frequency radiation before the high-frequency origin time of the event. While these studies have established that some oceanic transform earthquakes have anomalously long duration seismic sources, they were prevented from characterizing the source process over the entire seismic band by the sparse distribution of high-quality broadband seismic stations before the mid 1990s and the typically large distances between these stations and oceanic transform faults.

The most well recorded example of a slow, oceanic transform fault event is the April 28, 1997 earthquake on the Discovery II transform near Prince Edward Island, south of Africa [*McGuire and Jordan* 2000] . This event met Okal and Stewart's criteria for being anomalous in that it was m_b 5.7 and M_w 6.8 and its P-wave arrivals clearly indicated a complicated long-duration source. However, much more can be learned about

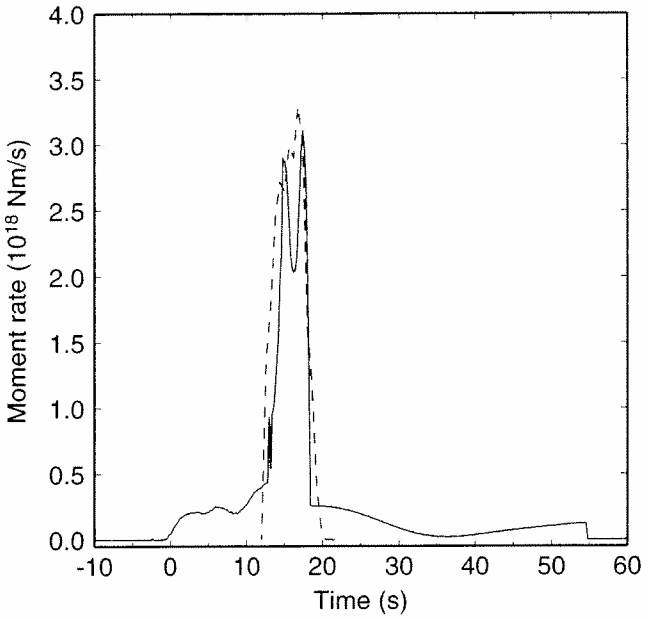

Figure 2. Source time functions for the 1997 Prince Edwards (solid line, [McGuire and Jordan, 2000]) and the 1994 Northridge (dashed line, [Wald et al., 1996]) earthquakes. Zero on the x-axis is the high-frequency origin time of the Prince Edwards event, and the Northridge STF has been shifted along the x-axis to overlap the Prince Edwards mainshock.

its source process than previous events because it was recorded by a temporary array of quiet, broadband stations in southern Africa [*James et al.,* 1998] at an epicentral distance of only about 20°. The P-waves recorded at this array clearly show an unusual low-frequency character relative to ordinary earthquakes (Figure 1). They begin with a low-frequency ramp that lasts about 15 s before the arrival of significant high-frequency energy (Figure 1). This type of low-frequency ramp is not observed for typical earthquakes of this size, such as the 1994 Northridge event (Figure 1) or other magnitude 6 earthquakes on the Discvoery II transform [*McGuire and Jordan* 2000]. We determined a STF for this earthquake that was consistent with the data ranging in period from 1000s to .5s. This STF reproduces the near lack of high-frequency radiation in the first 15 s, the low-frequency surface-wave amplitudes, and the precursory ramp in the low-frequency P-waveforms [*McGuire and Jordan* 2000]. This STF is compared to the 1994 Northridge event's STF [*Wald et al.,* 1996] in Figure 2. The 1997 Discovery II event had a compound STF comprised of a long duration (~30 s) slow component that was about M_w 6.3 and an ordinary earthquake that was similar in size and duration (~5 s) to the Northridge event. Because the smooth slow-component began rupturing before the ordinary subevent, it generated the precursory ramp seen in the low-frequency P-waveforms shown in Figure 1.

Another event that showed a low-frequency precursory ramp prior to the arrival of high-frequency P-wave energy was the 1994 M_w 7.1 Romanche transform earthquake in the central Atlantic. While this event was recorded much less clearly than the Prince Edward's Island earthquake, a stack of the 6 lowest-noise P-wave recordings did reveal a low-frequency precursor that exceeded the background noise level and began about 90 s before the high-frequency arrival times [*McGuire et al.,* 1996]. Additional evidence for this long-duration slow-component was obtained from low-frequency measurements of the source amplitude spectrum made using surface-wave and free oscillation techniques [*McGuire et al.,* 1996]. These two types of data suggested the presence of a 200 s long slow component that began radiating low-frequency energy prior to the onset of the main shock.

While the time domain observation of low-frequency, precursory arrivals for the Romanche and Prince Edward Island earthquakes can be clearly interpreted as evidence for a slow-source process, the complementary spectral observations are more ambiguous owing to their dependence on an assumed earth-model. For instance, *Abercrombie and Ekström* [2001] presented results which claim that the low-frequency spectral anomalies observed for the 1994 Romanche event were an artifact of using the PREM elastic structure [*Dziewonski and Anderson*(1981)] (which has a 21 km thick crust) to calculate the synthetic seismograms on which the measurements depend. *Abercrombie and Ekström* [2001] found that synthetic seismograms calculated using a thinner (6.5km) crust (more appropriate for an oceanic region) lead to an almost flat low-frequency amplitude spectra which implies an absence of a slow-component. This absence of a slow component would be in disagreement with the P-waves. In Figure 3A-B we present measurements of the low-frequency source-spectra for the 1994 event that were made using synthetic seismograms calculated for the PA5 elastic structure (Pacific basin velocity model with a 6.8 km crust)[*Gaherty et al.,* 1996] combined with the PREM attenuation model. This amplitude spectrum shows a distinct increase in amplitude below about 8 mHz. While this low-frequency amplitude anomaly is slightly reduced relative to the result we obtained with the PREM elastic structure, there is still a clear break in the amplitude spectra indicating a compound source. Inversion of these spectra combined

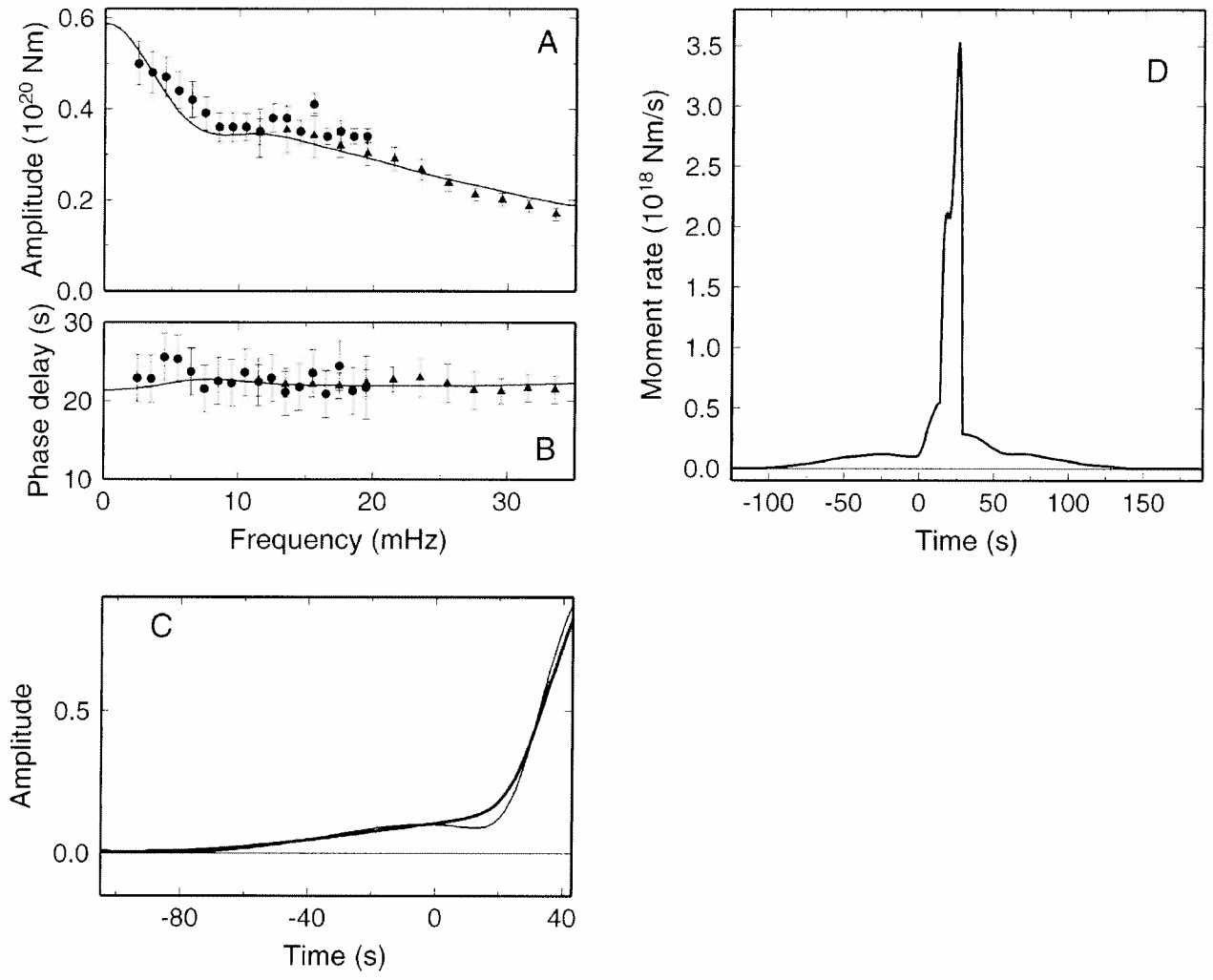

Figure 3. (A) Amplitude and (B) phase-delay spectra for the 1994 Romanche Transform earthquake determined using the oceanic velocity structure PA5. Points are estimates with one-sigma error bars obtained from propagation-corrected spectra averaged overa global network of 32 broadband stations; wave types used in the measurements are spheroidal free oscillations (solid circles), and long-period body wavetrains (solid triangles). Solid lines are the spectra obtained by Fourier transforming the source time function in panel D. The phase-delay spectrum is referenced to the NEIC high-frequency origin time, which corresponds to the initiation of event A. The spectra were made with synthetic seismograms for a point-source at 18 km depth with a focal mechanism (strike 85, dip 84, slip -161) determined from low-frequency inversion. (C) Comparison of the observed P-wave stack from McGuire et al. [1996] (thick line) with a synthetic seismogram (thin line) computed for the source time function in panel D. (D) Solid line is the source time function obtained by the joint inversion of the spectral-domain data in panels A and B and time-domain data in panel C.

with the low-frequency P-waveform stack (Figure 3c) yields a STF that is consistent with both types of data (Figure 3D). This STF shows a compound nature similar to the Discovery II event (Figure 2) in that it is comprised of both a (~200 s long) slow component and a (~20 s long) ordinary M_w 7 earthquake. Thus, the source-spectra determined for an oceanic velocity model are consistent with the low-frequency precursor seen in the P-wave stack. The difference between our result and that of *Abercrombie and Ekström* [2001] may be due to the difference in measurement technique (note the divergence of our PREM spectra from theirs at around 10

mHz in their Figure 4) or in the differences in oceanic velocity/Q models used. We find that the precursor seen in the P-waves for this event is consistent with the amplitude spectra calculated for an oceanic model. The STF determined from the oceanic model is very similar in its compound event character to the much more well constrained STF for the Prince Edwards event, suggesting that they result from unusual but similar source processes.

Preliminary directivity studies of the 1994 Romanche and 1997 Prince Edwards Island events indicated that they may have ruptured multiple fault-planes. Hence, there may be a connection between slow rupture and the broadly distributed deformation observed at Romanche on geologic time-scales. In this paper we present more detailed studies of the directivity in these ruptures and examine the relationship between these slow earthquakes, the background seismicity, and the long-term evolution of complicated multi-fault transform boundaries.

4. SEISMICITY OF THE ROMANCHE TRANSFORM

We began studying the current deformation of the Romanche transform by relocating all earthquakes in the ISC catalog from 1964 to 1996 using the clustered event algorithm of *Jordan and Sverdrup* [1981] . This technique produces estimates of the relative locations of the events that are independent of common path anomalies as well as an estimate of the absolute position of the seismicity cluster. We divided the Romanche transform into four overlapping regions (-25.5°E to -21°, -22.5° to -19°, -20° to -17.5°, and -18° to -15.5°) and simultaneously relocated all the events within a region. All event depths were constrained to 10 km, and only events with 30 or more P and PKP arrival times were used. The results (Plate 1) show that the vast majority of seismicity is concentrated into a series of seismicity clusters within the main transform valley (valley C). There are two notable gaps in the seismicity centered at -23° and -21° which stretch for about 100-150 km along the strike of the fault. Another interesting feature of the seismicity is that it extends 50-100 km beyond the eastern RTI (Plate 1D). This cluster of events, which is centered around (-16.5°E, 0.5°N), is dominated by a series of events in September 1993 including a m_b 5.2 (18 Sept., 1993) and an m_b 5 .4 (21 Sept., 1993) event. The extent of seismicity past the RTI agrees well with models of the geoid anomalies over fracture zones, suggesting that transform faults may take up to 4 Ma after passing the RTI to completely lock [*Wessel and Haxby,* 1990]. The presence of these moderately sized events past the end of the active plate boundary may also result from the unusual oblique nature of the eastern RTI.

While the vast majority of seismicity locates within the transform valley, there are several events located outside this zone. Most of these are small (m_b 4.5) events whose 95% confidence ellipsoids nearly overlap the main fault valley. Hence they do not represent a significant amount of distributed deformation. However, there are several large earthquakes that locate near the 'paleo-transform' faults labeled A and B in Figure 1. The 5 May, 1987, (M_w 6.0) event location is shown in Plate 1C. This large event has over 150 P-wave arrival time picks and good azimuthal coverage resulting in location uncertainties of $\leq$ 10 km. Its location is within the fault valley (B) suspended in the northern transverse ridge. This fault, identified by *Bonatti et al.* [1994] as probably having been the primary trace of the Romanche transform until about 8-10 Ma, evidently can still produce a magnitude 6.0 strike-slip earthquake.

We also included arrival time picks of the largest subevents in the M_w 7 Romance transform earthquakes of 5 August, 1971 and 14 March, 1994. Both of these events began with a small preshock that was followed by a much larger mainshock. Picking the P-wave arrivals from later arriving subevents is generally not possible for shallow earthquakes owing to the interference from depth phases. However, the mainshocks of these earthquakes were approximately 10 times larger than the preshocks, making their first arrivals distinguishable from the preshock coda [*McGuire et al.,* 1996]. *Forsyth et al.* [1986] found that the mainshock of the 1971 event occurred 10 s later than and was located 60 km to the NNW of the preshock. Using arrival time picks made on WWSSN records (Table 1), our relative location produced almost identical results to those of *Forsyth et al.* [1986] . The 1971 preshock (labeled 71A in Plate 1A)is located in the main transform valley while the mainshock (labeled 71B) is located 58 km to the NNW. The location of the mainshock is inconsistent with it rupturing the main transform and suggests that this subevent ruptured either paleotransform A or B. The 1994 event also had two sets of pickable arrivals corresponding to the subevents that begin at 0 s (the preshock labeled 94A if Plate 1A) and at 15 s (the mainshock, labeled 94B) in Figure 3. Using our travel-time picks for the preshock and mainshock of the 1994 event [*McGuire et al.,* 1996] we also find that the location of its mainshock is consistent with paleotransforms A and B but not with the Romanche PTDZ.

Table 1. 5 August 1971 Mainshock Delay Times from WWSSN seismograms

Station	Azimuth (deg.)	Epicentral Distance (deg.)	B-A Time (s)
BUL	115	53	13.6
GRM	131	56	12.6
SDB	113	38	11.0
PRE	121	54	15.0
NAI	91	59	10.6
SHI	59	77	10.6
AAE	79	62	11.6
COP	21	63	9.6
EIL	56	62	10.1
ESK	13	58	11.3
HLW	54	59	10.2
JER	53	63	10.0
KON	17	65	10.6
KBL	56	91	9.6
NUR	22	71	9.6
KTG	00	71	7.8
QUI	270	56	6.0
SJG	296	47	7.1
LPA	221	48	12.1
GOL	310	85	6.9
ATU	43	57	9.9
KEV	16	77	10.2
BEC	315	51	6.0
DAL	304	77	6.6
JCT	301	78	6.5
LUB	304	82	7.2
WIN	121	45	15.0

Recently, a hydrophone array on the northern mid-Atlantic Ridge has begun monitoring microseismicity in the Atlantic basin using T-phase arrivals [*Smith et al.*, 2000; *Bohnenstiehl et al*, 2000]. This array located about 10 micro-earthquakes during the year May 1999 to May 2000, just north of the northern transverse ridge, in fault valley A, primarily in the eastern half of the transform [*Smith et al.*, 2000]. Thus, while the vast majority of moderate (M_w 4-5) seismicity and several large (M_w ~7) events occur along the main transform, it appears from P-wave travel-time based locations and T-phase locations of micro-seismicity, that at least one of the northern paleotransforms is still seismically active.

5. SECOND MOMENTS OF SLOW-EARTHQUAKES

Determining the space-time rupture properties of earthquakes that are only recorded teleseismically is a difficult process. The subevent locations of large earthquakes discussed in the previous section and in *McGuire et al.* [1996] and *McGuire and Jordan* [2000] suffer from a potential source of bias owing to the difficulty in distinguishing later arriving P-waves from depth phases. Attempts to determine detailed maps of slip as a function of space and time using teleseismic body-wave data are fundamentally non-unique even when there is little error in the theoretical Green's functions utilized by the inversion [*Ihmle*, 1998]. In order to reduce the number of unknown parameters, these inversions are often forced to constrain the rupture to an *a priori* fault-plane with a specified rupture velocity rather than explicitly determining the associated quantities such as rupture azimuth. *Ihmle* [1998] showed that the non-uniqueness in these problems is associated with the often arbitrary choice of the spatial smoothing parameter. Thus even when an inversion fits the data very accurately at high-frequencies (1 Hz), the result at best only gives a very general picture of the rupture [*Ihmle*, 1998].

Abercrombie and Ekström [2001] inverted teleseismic body-waves at frequencies up to 1 Hz for a detailed description of the 1994 Romanche event's rupture and found a moderately good fit for a rupture model that was constrained to a single fault with a strike of 82°. They claimed that there was no evidence for a multi-fault rupture in this event. However, their rupture model produces early arrival times for the main P-wave group arrival at station to the SW (LPAZ and NNA, *Abercrombie and Ekström* [2001] in their Figure 3) suggesting that a rupture azimuth more towards the NE than 82°, which would correct this mismatch, may be a possibility.

Unfortunately for large earthquakes on oceanic transform faults, finite-fault inversions are significantly more complicated than the deep earthquake case investigated by *Ihmle* [1998] . The teleseismic seismograms resulting from a strike-slip source underneath a water-layer are extremely sensitive to the topography of the rock-water interface [*Yoshida*, 1992] owing to changes in the take-off angle of the depth-phases and their water-layer reverberations. These effects are significant for seafloor slopes as small as 0.5 degrees [*Wiens*, 1987] and are clearly important for the source region of the 1994 Romanche earthquake which has topographic variations of over 3 km on length-scales of less than 50 km [*Searle et al*,, 1994]. For a typical water-layer thickness, the teleseismic Green's functions become significantly complicated at periods shorter than about 10-20 s. Thus unless a realistic model of bathymetry is incorporated

into the Green's function calculation, it is preferable to determine information about an oceanic transform earthquake's space-time distribution from data at periods longer than this range. This low-frequency restriction prohibits resolution of the detailed spatial dependence of slip.

Certain aspects of an earthquake's space-time rupture history can be robustly determined from low frequency waveforms (periods $\geq$ 20 s) by inverting for a set of quantities known as the second degree polynomial moments of the source distribution [*McGuire et al.*, 2001]. The second-moments include the variances of the moment-release distribution in 4-D space-time and hence are measures of the extent of the rupture, i.e., length, width, duration, and velocity. The two second moment quantities that provide information on the spatial distribution of moment release are the second spatial moment, $\boldsymbol{\mu}^{(2,0)}$, and the mixed-moment between space and time, $\boldsymbol{\mu}^{(1,1)}$:

$$\hat{\boldsymbol{\mu}}^{(2,0)} = \int\int \dot{f}(\mathbf{r},\mathbf{t})\,(\mathbf{r}-\mathbf{r_0})(\mathbf{r}-\mathbf{r_0})^{\mathrm{T}}\,\mathbf{dV\,dt} \qquad (1)$$

$$\hat{\boldsymbol{\mu}}^{(1,1)} = \int\int \dot{f}(\mathbf{r},\mathbf{t})\,(\mathbf{r}-\mathbf{r_0})\,(\mathbf{t}-\mathbf{t_0})\,\mathbf{dV\,dt}\,. \qquad (2)$$

Where $(\mathbf{r_0}, t_0)$ are the centroid location and time, $\dot{f}(\mathbf{r},t)$ is a scalar function describing the spatial and temporal dependence of seismic moment release, and the coordinates (r,θ,ϕ) correspond to the radial direction, colatitude, and longitude.

Following *Backus* [1977] and *Silver and Jordan* [1983] , the 2nd moments can be interpreted in terms of the characteristic dimension, $x_c(\hat{\mathbf{n}})$, of the slip distribution in a direction $\hat{\mathbf{n}}$, the characteristic duration τ_c, the characteristic length L_c, the characteristic (or apparent rupture) velocity v_c, and the average velocity of the instantaneous spatial centroid, $\boldsymbol{v_0}$:

$$x_c(\hat{\mathbf{n}}) = 2\sqrt{\hat{\mathbf{n}}^{\mathrm{T}}\cdot\left(\hat{\boldsymbol{\mu}}^{(2,0)}/\mu^{(0,0)}\right)\cdot\hat{\mathbf{n}}}, \qquad (3)$$

$$\tau_c = 2\sqrt{\hat{\mu}^{(0,2)}/\mu^{(0,0)}}\,, \qquad (4)$$

$$v_c = L_c/\tau_c\,,\ \mathbf{v_0} = \hat{\boldsymbol{\mu}}^{(1,1)}/\hat{\mu}^{(0,2)}, \qquad (5)$$

where M_0 is the seismic moment and $x_c(\hat{\mathbf{n}})$ has its maximum value, L_c, when $\hat{\mathbf{n}}$ corresponds to the eigenvector associated with the largest eigenvalue of $\hat{\boldsymbol{\mu}}^{(2,0)}$. The second largest eigenvalue of $\hat{\boldsymbol{\mu}}^{(2,0)}$ corresponds to the characteristic rupture width W_c. The vector $\hat{\boldsymbol{\mu}}^{(1,1)}$ specifies the average velocity of propagation of the instantaneous centroid, $\mathbf{v_0}$, i.e. the average directivity. The eigenvector of $\hat{\boldsymbol{\mu}}^{(2,0)}$ corresponding to L_c is not constrained to have the same orientation as $\mathbf{v_0}$. For instance, a large subduction zone thrust earthquake that nucleates at the base of the seismogenic zone and propagates towards the trench as well as bilateraly along strike could have its longest dimension along strike while its average directivity is updip. Thus, L_c and $\mathbf{v_0}$ would be orthoganal. However, for a predominantly unilateral rupture on a rectangular strike-slip fault, L_c and $\mathbf{v_0}$ are usually nearly parallel.

We have developed a method for determining the second moments of earthquake space-time distributions from low-frequency, teleseismic surface and body-wave data [*McGuire et al.*, 2001]. This method uses the perturbations to the low-frequency wavefield caused by the constructive and destructive interference resulting from the finite extent of the seismic source to determine the second moments. These perturbations are measured as amplitude anomalies relative to synthetic seismograms that are calculated for a point-source. We invert for 20 parameters that specify the moment-tensor (zeroth order moment), centroid location (first order moment), and the independent elements of the second-degree moments of an earthquake moment-release distribution. We are often able to determine the second moment quantities, such as L_c and $\mathbf{v_0}$, to within the level of uncertainty associated with different finite-fault inversions of local strong-motion data [*McGuire et al.*, 2001]. Thus, while the second moments only provide a low-order description of the rupture, they are clearly resolvable for large oceanic transform fault earthquakes. We have estimated the second moments of the space-time distributions of moment-release in three large earthquakes on the Romanche and Discovery II transform to investigate the possibility that some of these events ruptured multiple sub-parallel faults.

5.1. *The 1994 and 1995 Romanche Earthquakes*

The western portion of the Romanche transform recently ruptured in two large events, the March 14, 1994, M_w 7.0, and the May 18, 1995 M_w 6.8, earthquakes. We measured the phase-delay and amplitude-reduction times relative to synthetic seismograms for the 1st and 2nd orbit Rayleigh waves, and P-waves at global teleseismic stations using the Generalized Seismological Data Functional (GSDF) technique of *Gee and Jordan* [1992] . The synthetic seismograms were calculated by mode-summation for the PREM earth model [*Dziewonski and Anderson*, 1981], corrected for

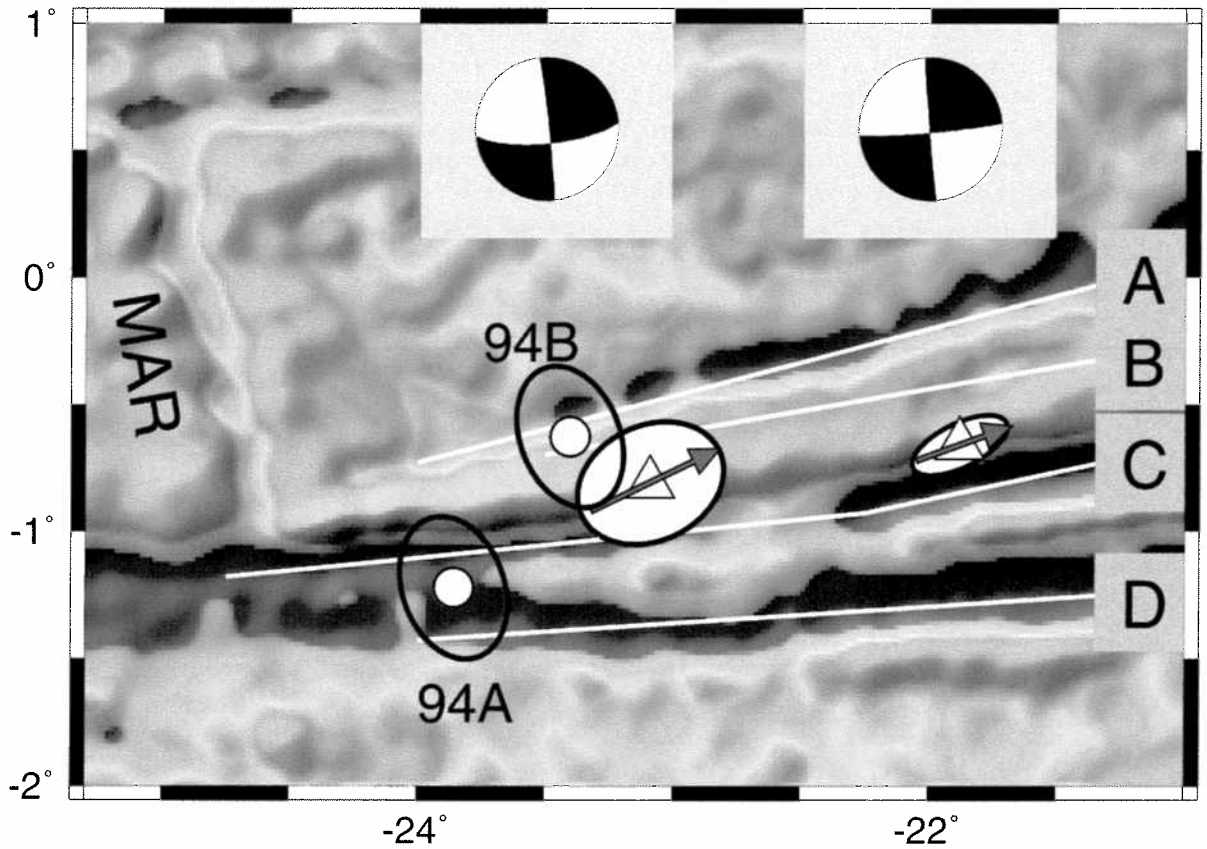

Plate 2. Map showing the western portion of the Romanche transform. Colors and white lines denote the gravity field and fault locations as in Figure 1. Focal mechanism inserts show the solutions for the 1994 and 1995 events. The white circles surrounded by black ellipses denote the locations and 95% confidence regions for the initial and main high-frequency subevents of the 1994 event determined in section 2. The triangles show the centroid locations of the 1994 (23.09±.10°W, 0.81±.01°S) and 1994 (21.88±.01°W, 0.66±.01°S) events. The white ellipses with black borders that are centered on the centroid locations denote the map-view projection of the characteristic rupture volume defined by our estimates of the 2nd spatial moment for each earthquake. The red vectors denote the average directivity vector specified by the mixed space-time moment. The length of these vectors has been scaled to be equal to $\tau_c v_0$.

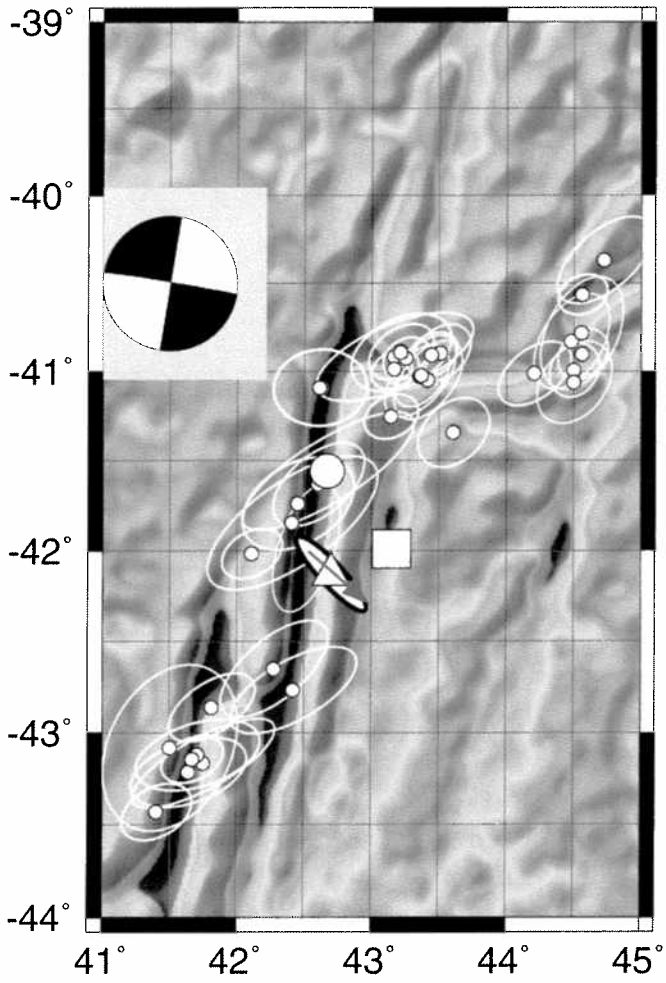

Plate 3. Map of the N-S trending Discovery II transform in the Southwest Indian Ocean. Colors are the satellite altimetric free-air gravity field as in Figure 1. Relocated seismicity from the 1965-1996 ISC catalog is shown as small circles with 95% confidence ellipsoids. The large circle and square are the locations of the epicenter and mainshock of the 1997 event determined in McGuire and Jordan [2000]. The triangle shows the event's centroid location. The white ellipse with black border denotes the map-view projection of the characteristic rupture volume degined by our estimate of this event's 2nd spatial moment. The red vector denotes its average directivity as specified by the mixed space-time moment. The vector's length has been scaled to equal $\tau_c v_0$.

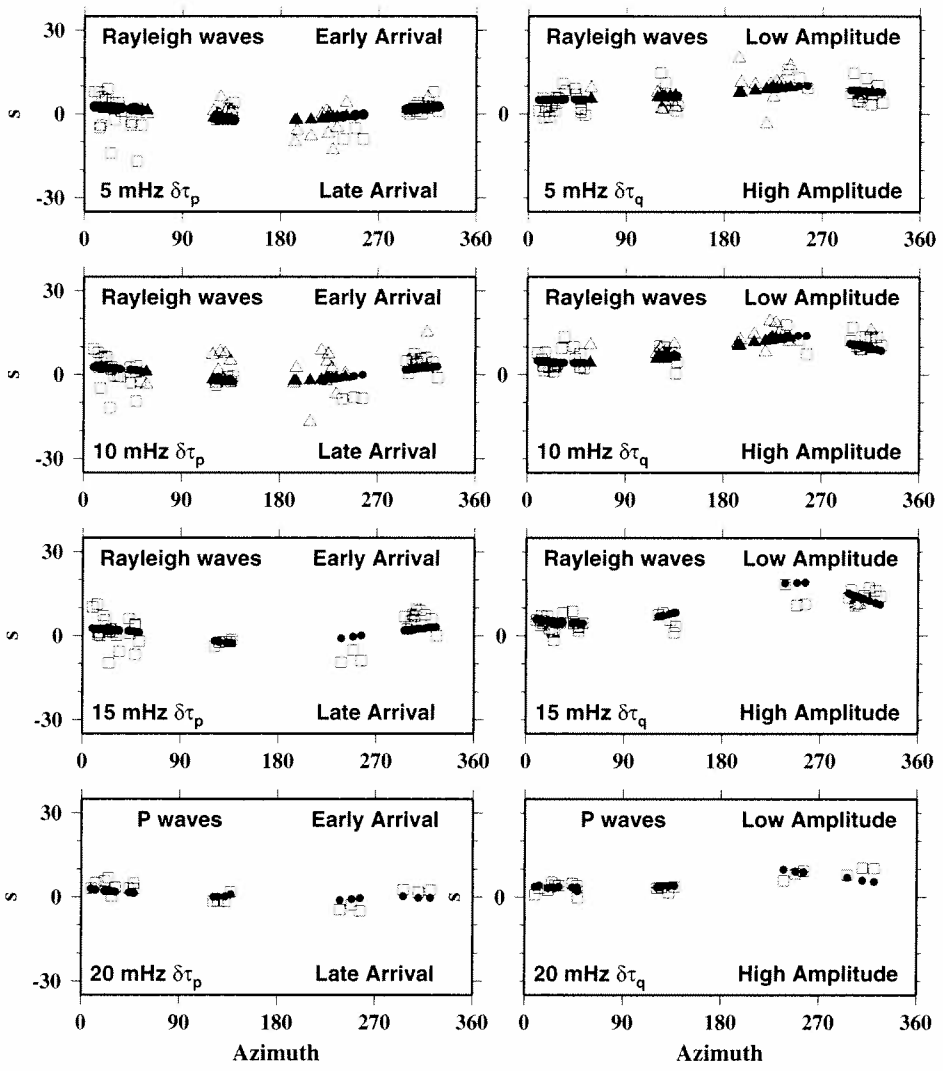

Figure 4. GSDF measurements of the 1994 Romanche transfrom earthquake at 5, 10, 15, and 20 mHz. Open squares denote R1 and P-wave measurements, and open triangles denote R2 measurements. Filled symbols indicate the fit to the date produced by the estimates of the 0th, 1st, and 2nd moments in Tables 2, 3, and 4.

three-dimensional elastic structure using the degree-12 aspherical model of *Su and Dziewonski* [1994] and the approximations of *Woodhouse and Dziewonski* [1984] . We also corrected fundamental modes above 7 mHz for smaller scale heterogeneity using the degree-40 phase velocity maps of Ekstrom et al., [1997]. The source is specfied by an initial centroid location, centroid time, and moment tensor corresponding to the Harvard CMT solution for each event [*Dziewonski et al.,* 1999]. Measurements of second orbit Rayleigh waves, which have greater contamination from unmodeled propagation effects than R1, were necessary to achieve sufficient azimuthal coverage to the south and southwest (where the P-waves have insufficient coverage). The measurements (Figures 4 and 5) for both events show phase-delay times, $\delta\tau_p(\omega)$, that are roughly independent of azimuth indicating that the CMT centroid locations were approximately correct for both events. The amplitude reduction times, $\delta\tau_q(\omega)$, show a systematic increase with frequency for Rayleigh waves that leave to the west or southwest of the source. These positive values, corresponding to a reduction in data amplitude relative to point-source synthetics, indicate that the rupture propagated primarily to the E or NE.

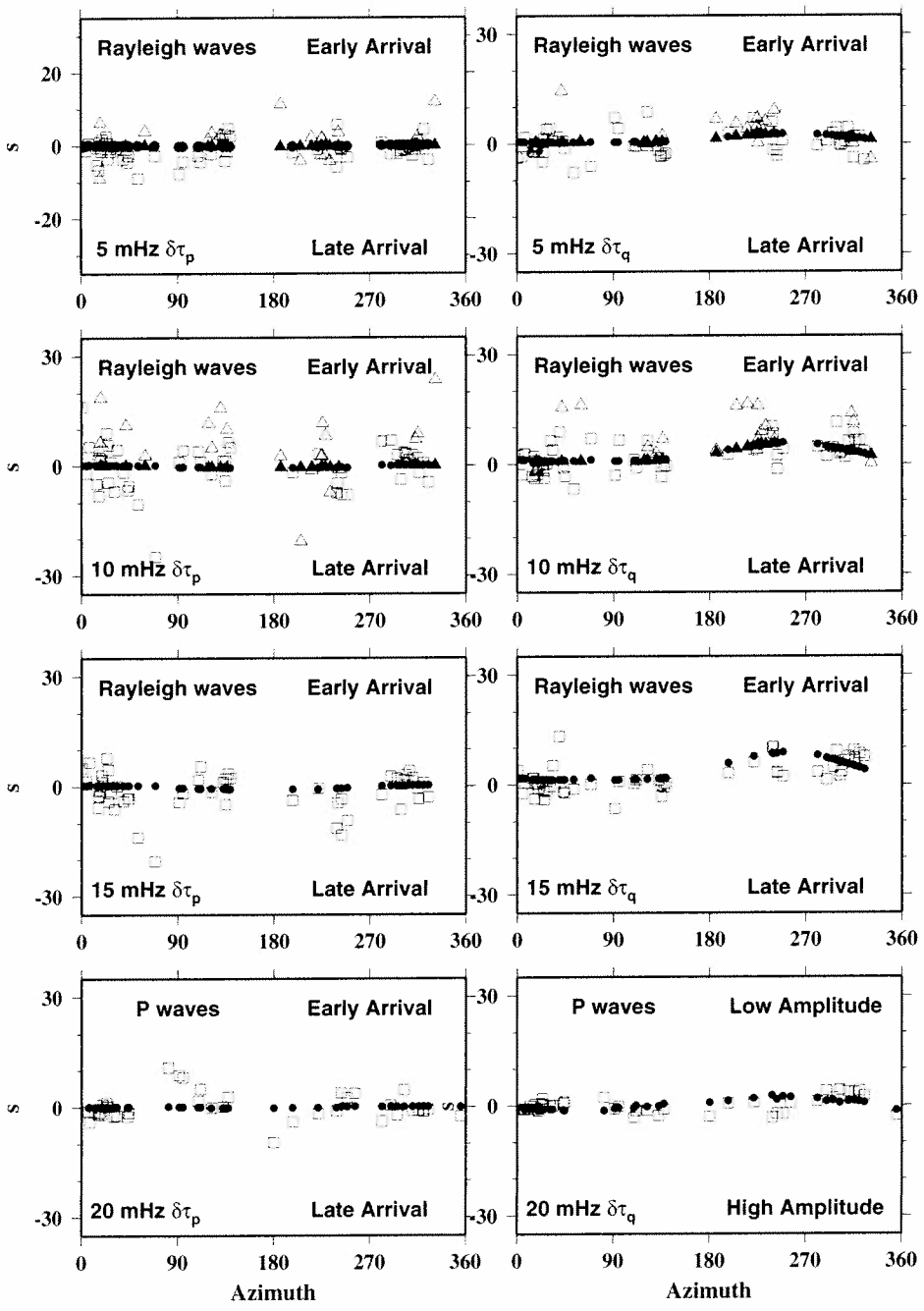

Figure 5. GSDF measurements of the 1995 Romanche transform earthquake. Symbols are the same as in Figure 5.

Inverting the measurements in Figures 4 and 5 for the 0th, 1st, and 2nd moments of the rupture distribution yielded the estimates in Tables 2, 3, 4, and 5. The measurement and inversion procedures were iterated until the CMT parameters were stable. For the 1995 event, the 2nd moments correspond to a characteristic duration, τ_c, of 13±5 s, a characteristic rupture length, L_c of 45±6 at an azimuth of 64°, an average centroid velocity, $\mathbf{v_0}$ of 3.4±5 km/s at an azimuth of 70°. For the 1994 Romanche event, the 2nd moments correspond to

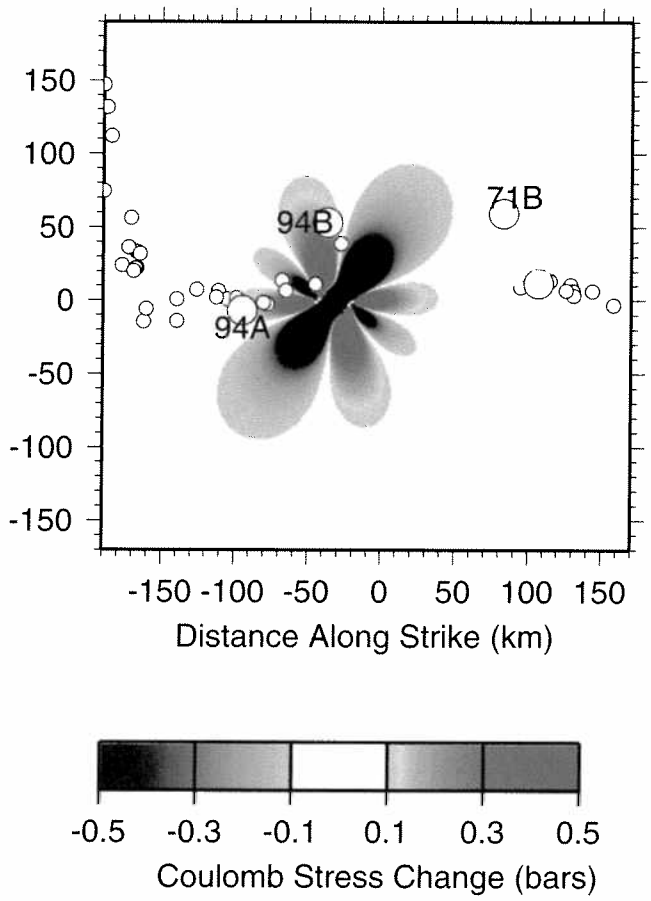

Plate 4A. Map view showing the changes in Δ_f for run #5 of Table 6. The small circles denote the seismicity locations from Figure 1A. The large circles denote the subevent locations for the 1994 and 1971 events whon in Figure 1. The horizontal axis denotes distance along the direction of strike of the main transform. The source and receiver faults were assumed to be vertical faults with this strike. The origin of the co-ordinate system is at 23.0°W and 1.0°S.

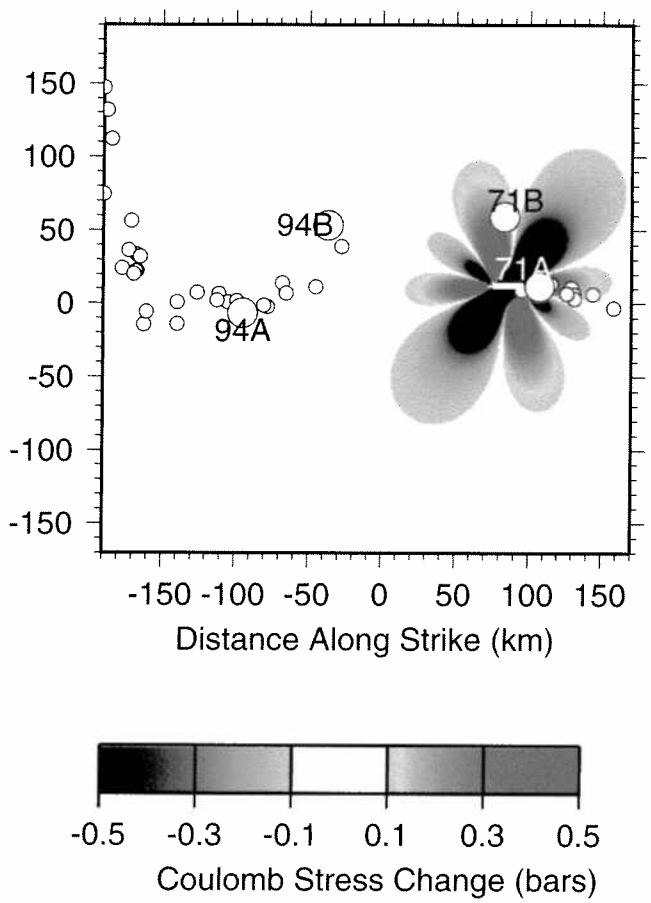

Plate 4B. Map view showing the changes in Δ_f for run #5 of Table 6, but shifted to be aligned with the 1971 event's subevents. Same as Figure 11.

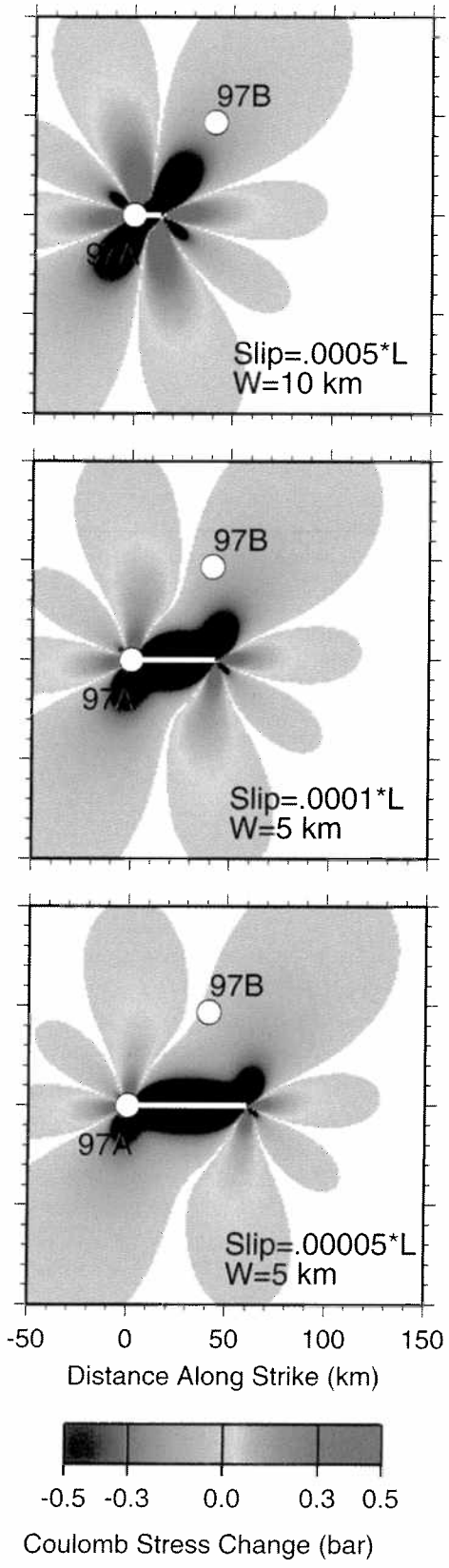

Plate 4C. Plot showing the changes in Δ_f resulting from the 1st 15 s of the 1997 Prince Edward Island slow earthquake. The large circles denote the subevent locations for the slow component (97A) and mainshock (97B). The horizontal axis denotes distance along the direction of strike of the main transform. The source and receiver faults were assumed to be vertical faults with this strike. The origin of the co-ordinate system is at the epicenter of the slow component.

Table 2. Moment Tensor inversion results

earthquake	rr	$r\theta$	$r\phi$	$\theta\theta$	$\theta\phi$	$\phi\phi$
94 Romanche	-.02	.08	-.07	-.0004	-.11	-.37
95 Romanche	-.004	.0068	-.064	.0046	-.0133	-.202
97 Prince Edwards	-.011	.054	-.043	-.0008	-.0067	.14

values are in units of 10^{20} Nm

Table 3. 1st moments inversion results

earthquake	$\mu^{(0,1)}$ time	$\hat{\boldsymbol{\mu}}^{(1,0)}$ lat.	lon.	depth
94 Romanche	04:30:33.2±.1	0.81±.01°S	23.09±.01°W	10.0*
95 Romanche	00:06:37.4±.3	0.66±.01°S	21.88±.01°W	26.0±1.2
97 Prince Edwards	-12:07:47.7±.1	42.13±.01°S	42.70±.01°E	8.6±1.2

Errors are ±2 standard deviations. * indicates the depth was fixed in the inversion.

a τ_c of 22±2 s, a L_c of 66±8 km at 65°, and a $\mathbf{v_0}$ of 2.8±.9 km/s at 64°. The centroid locations, characteristic source volumes, and directivity vectors for the two earthquakes are shown in Plate 2.

The mixed-moment between space and time that defines $\mathbf{v_0}$ is the most well resolved of the 2nd moments due to the large effect it has on the amplitudes of surface and body waves. The directivity vector, $\mathbf{v_0}$, for the 1995 event is nearly aligned with the strike of the main transform in this region (an azimuth of 70° vs 80°). The strike of the main Romanche transform undergoes a series of discrete changes along its length [*Bonatti et al.*, 1994]. One of these changes occurs at about 22°W, such that in the region of the 1994 event the fault strikes almost E-W while near the centroid of the 1995 event its strike has rotated by ~ 10° towards ENE [*Bonatti et al.* 1994; Figure 15]. Thus, if both events ruptured only the main transform (fault C), we would expect the 2nd moments of the 1994 event to have an orientation closer to E-W than those of the 1995 event, but we observe the opposite. The estimate of $\mathbf{v_0}$ for the 1994 event has an orientation, N64°E, that is at a significant angle (~ 25°) to the strike of the main-transform valley (Plate 2). While the ~10° difference between the 1995 event's directivity vector and the strike of the main transform may result in part from estimation error, the ~ 25° difference for the 1994 event is larger than the scatter we typically observe for strike-slip faults [*McGuire et al.*, 2001b]. It is also larger than the mismatch observed for the 1995 M_w 7.2 Gulf of Aqaba event, the rupture of which jumped between parallel segments of the Dead Sea Transform Fault [*Pinar*, 1997; *Klinger et al.*, 1999] creating a ~ 15° mismatch vetween $\mathbf{v_0}$ and the strike of it's fault-plane [*McGuire et al.*, 2001]. Thus, this mismatch for the 1994 event appears to indicate a complex rupture.

Table 4. 2nd moments inversion results

earthquake	$\mu^{(0,2)}$	$\hat{\boldsymbol{\mu}}^{(1,1)}$ r	θ	ϕ
94 Romanche	123±11	0±7	-155±51	313±39
95 Romanche	39±15	5±7	-45±28	126±19
97 Prince Edwards	20±5	-7±4	98±14	112±11

All values have been normalized by the moment of the event, the units of $\hat{\mu}^{(0,2)}$ are s^2, $\hat{\boldsymbol{\mu}}^{(1,1)}$ are km s. r is the radial direction, θ is co-latitude, ϕ is longitude. Errors are ±1 standard deviation.

Table 5. 2nd moments inversion results

	$\hat{\mu}^{(2,0)}$					
	rr	rθ	rϕ	$\theta\theta$	$\theta\phi$	$\phi\phi$
94 Romanche	7±6	-14±25	10±51	708±306	-181±225	1013±221
95 Romanche	27±10	41±27	2±28	148±180	-169±108	420±102
97 Prince Edwards	15±2	13±3	-12±11	958±374	808±310	839±336

The NE-SW orientation of $\mathbf{v_0}$ (the second-order moment) for the 1994 earthquake is inconsistent with rupture on a single, E-W striking fault, such as the E-W nodal plane of the earthquake focal mechanism (zeroth-order moment). Additionally, the 1994 centroid location (1st-order moment) lies in between fault valleys B and C, although the uncertainty in this position is relatively large. The only type of source model that can satisfy the observed 0th, 1st, and 2nd moments is one that involves right-lateral slip on two nearly parallel faults oriented approximately E-W and offset in such a way as to produce the observed 2nd moments. The subevent locations for the 1994 event indicate either fault A or B ruptured as well as fault C, with the slip on fault A or B occurring to the northeast and subsequent to the rupture of fault C. This type of source model can satisfy the observed moment-tensor because the B and C faults are sub-parallel. It can also satisfy the centroid location, which is intermediate between the two faults, and the NE directivity required by the second moments.

5.2. *The 1997 and 1998 Discovery II Earthquakes*

The 28 April, 1997, M_w6.8, Prince Edward Island earthquake that ruptured the Discovery II transform showed evidence from subevent locations that suggested directivity at a high angle to either fault-plane of the events moment-tensor, similar to the 1994 Romanche quake [*McGuire and Jordan*, 2000]. To investigate this directivity, we made measurements of the phase-delay time, $\delta\tau_p$, and amplitude-reduction time, $\delta\tau_q$, times of 1st orbit Rayleigh and P-waves (Figure 6) using the same technique described in the previous section. The low-frequency R1 measurements of $\delta\tau_p$ showed late arrivals at stations to the SW, indicating that the true centroid location was shifted in this direction. The low-frequency measurements of $\delta\tau_q$ for R1 had no systematic variation as a function of azimuth, indicating the starting moment-tensor was approximately correct. The higher frequency $P-$wave measurements showed systematic variations in both $\delta\tau_p$ and $\delta\tau_q$. The anomalies in $\delta\tau_q$, indicating large $P-$wave amplitudes at stations to the SE and small amplitudes at stations to the N and NW, increased in magnitude with frequency, as would be expected for a directivity affect. The $\delta\tau_p$ anomalies displayed no such increase, as would be expected for a shift in the true centroid location from the assumed location. To determine if the $\delta\tau_q$ anomalies were indeed a result of directivity, we compared the measurements for the 1997 event to measurements for a M_w 6.1 event in 1998 that also ruptured the Discovery II transform. The measurements of the 1998 event should indicate almost no directivity effects at these frequencies owing to its smaller seismic moment and corresponding spatial extent. The $\delta\tau_p$ measurements reveal a very similar azimuthal pattern to those for the 1997 event (Figure 7), indicating that these travel-time anomalies likely result from unmodeled 3-D heterogeneity rather than properties of the seismic source. On the other hand, the $\delta\tau_q$ measurements for the 1998 event show a nearly constant value as a function of azimuth and do not increase in amplitude with frequency (Figure 7). They have a mean of about -1±1.7s. The small scatter (±1.7 s) indicates that the $P-$wave measurements for sources in this region have relatively small anomalies in their amplitudes resulting from unmodeled propagation effects. Thus, the clear signal in the 1997 event's $P-$wave amplitude measurements, that indicates NW-SE directivity, appears to be a true source effect.

To quantify the directivity of the 1997 earthquake, we inverted the $\delta\tau_p$ and $\delta\tau_q$ measurements in Figure 6 for the 1st and 2nd moments of its rupture. The moment tensor was determined iteratively and then fixed at the value in Table 2. This slight change from the Harvard CMT moment tensor helped remove some of the $\delta\tau_p$ anomalies observed in Figure 6. The inversion results (Tables 3 and 4) correspond to a L_c of 83±16 km at an azimuth of 137°, a τ_c of 9±3 s, and a $\mathbf{v_0}$ of 7.6±17km/s at an azimuth of 131°. The large error bar on $\mathbf{v_0}$ ($\mathbf{v_0} = \hat{\boldsymbol{\mu}}^{(1,1)}/\hat{\mu}^{(0,2)}$) results from both the high uncertainty in τ_c and a strong negative correlation between the magnitudes of the estimates of $\hat{\mu}^{(0,2)}$ and

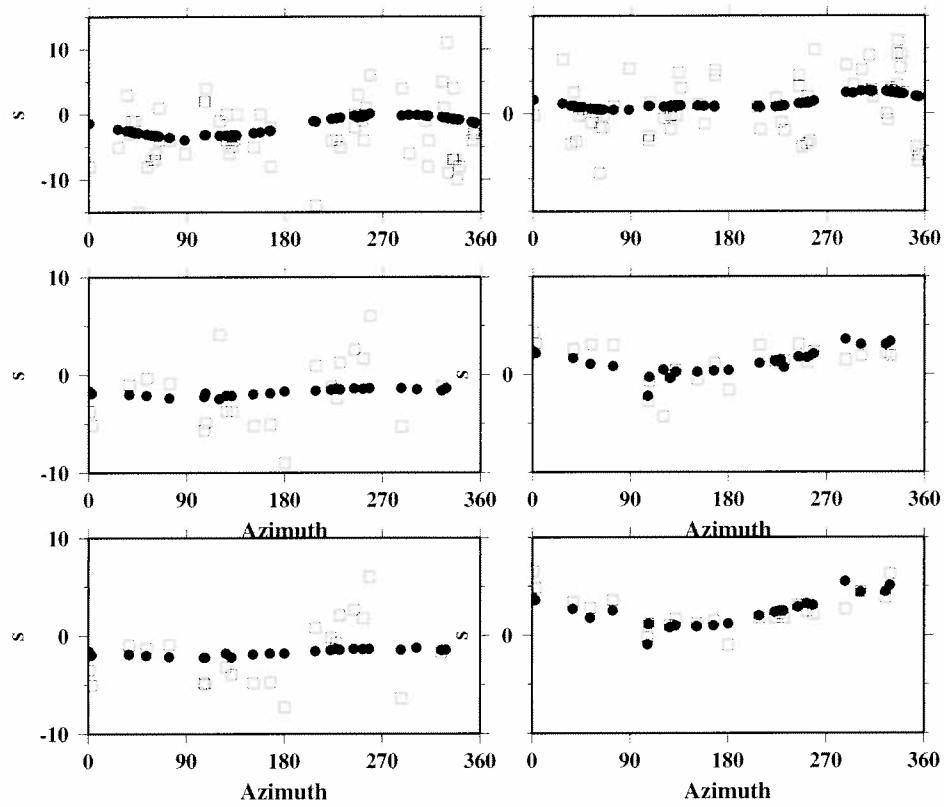

Figure 6. GSDF measurements of the 1997 Prince Edward Island earthquake at 10 mHz for R1, and 30 and 40 mHz for P-waves using the point-source parameters in Tables 2 an 3. Open squares denote measurements, and filled squares indicate the fit to the data produced by the estimates of the 0th, 1st, and 2nd moments in Tables 3 and 4. The measurements were made after a few iterations on the centroid moment-tensor parameter, hence there is relatively little signal left in the phase-delay measurements for the inversion to fit.

$\hat{\boldsymbol{\mu}}^{(1,1)}$. However, the estimates of $\hat{\boldsymbol{\mu}}^{(1,1)}$ have relatively small errors (Table 4) and indicate clear rupture propagation to the SE. This strong NW-SE directivity is at a high angle to the strike of the Discovery II transform (Plate 3) and the nodal planes of the moment tensor. Rupture propagation on a fault with a strike of 131° can be ruled out by this moment tensor. However, the orientation of the 2nd moments can be consistent with both the moment tensor, the centroid, and the directivity study if two sub-parallel N-S striking faults ruptured coseismically.

The Discovery II transform is a double transform connected by a small spreading segment at about 42.75°S. It also has an adjacent fault-valley to the east that can be traced for ~200 km on both sides of the northern ridge (Plate 3). This pair of valleys most-likely represents the fracture zone associated with a paleo transform fault since the SWIR shows no current offset at its projected intersection with these valleys. The 1997 earthquake began with a slow, smooth episode of moment release on the main transform that was followed ~12 s later by an ordinary mainshock (Figure 2). The location of the mainshock determined by *McGuire and Jordan* [2000] falls within the adjacent fault valley indicating that this fault ruptured in the 1997 mainshock (Plate 3). Thus both the NW-SE orientation of the 2nd moments and the directivity study in *McGuire and Jordan* [2000] suggest that the 1997 Prince Edward Island earthquake was a complex faulting event that ruptured both the main trace of the Discovery II transform and the adjacent paleotransform fault.

6. POSSIBLE CAUSES OF THE OFF-FAULT SUBEVENTS

The 1994 Romanche and 1997 Prince Edward Island earthquakes share many similarities. They consist of

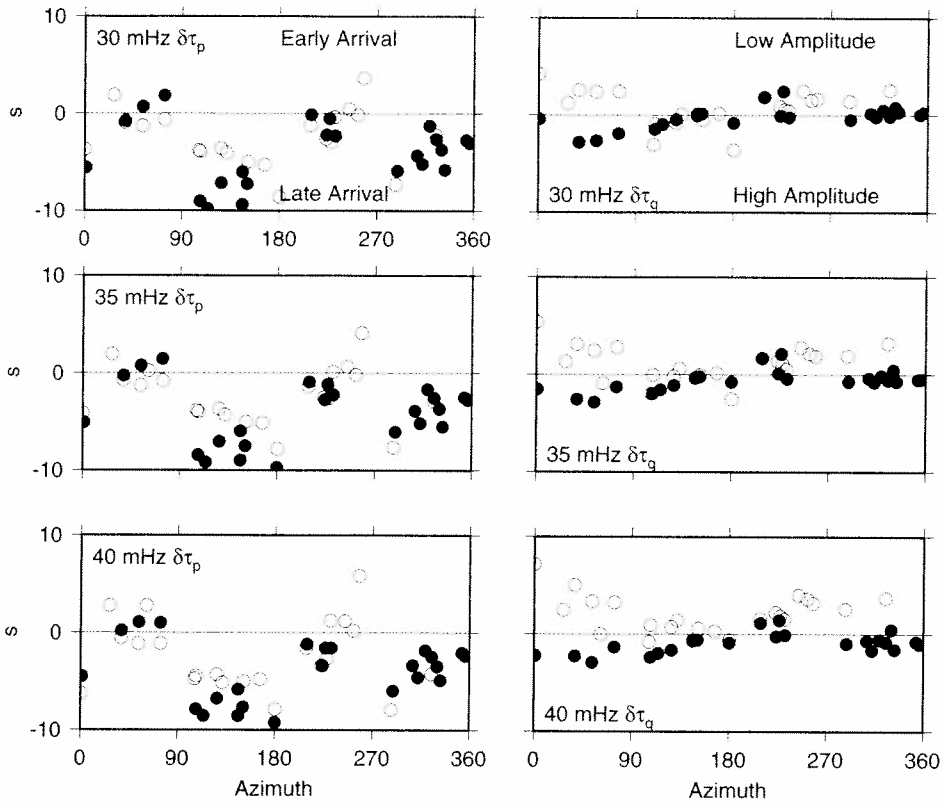

Figure 7. GSDF measurements of the $P-$waves for the 1997 and 1998 earthquakes on the Discovery II transform using the Harvard CMT point-source parameters (note this is the source of the difference between these measurements for the 1997 event and those in Figure 6). The solid circles are for the M_w 6.1, May 21, 1998 event and the open circles for the M_w6.8 April 28, 1997 event. Different station sets were available for the two time periods.

a sequence of right-lateral, strike-slip subevents that rupture not only the main transform faults but also sub-parallel faults about 40 km from each main transform. The events are compound earthquakes consisting of not only one or more ordinary rupture events, but also a smooth transient of longer duration that preferentially radiates energy at low-frequencies [*McGuire et al.*, 1996; *McGuire and Jordan*, 2000]. Both event sequences began with a slow rupture that was followed by the main high-frequency subevent on the adjacent paleo-transform. In the case of the Romanche event, precursory ramps in low-frequency $P-$ waveforms indicate that the slow component began rupturing at least 100 seconds before the high-frequency subevents, while for the Prince Edwards event, $P-$waveforms show that the slow component began approximately 10-15 seconds before the ordinary rupture. The observation that both events began with a slow component allows the possibility that the slow component may have triggered the unusual failure of the paleo-transform.

Coseismic rupturing of multiple widely separated faults in a single earthquake has been documented, most notably for the 1980, M_s 6.9, Irpinia, Italy, normal-fault earthquake. This event sequence propagated over at least three faults with each fault bringing the subsequent one closer to failure [*Nostro et al.*, 1997; *Belardinelli et al.*, 1999]. The last fault to rupture in this event was ~20-25 km from the preceding fault that triggered its failure. The likelihood of failure of a potentially triggered fault is usually evaluated in terms of the change in Coulomb failure stress, Δ_f [*King et al.*, 1994].

$$\Delta_f = \Delta\tau - \mu'\Delta\sigma \tag{6}$$

where μ' is the apparent coefficient of friction, $\Delta\tau$ and $\Delta\sigma$ (compression positive) are the change in shear and

normal stress on the triggered fault resulting from the slip on the source fault, respectively. Positive values of Δ_f promote failure; negative values inhibit failure. Δ_f can be considered as either a dynamic quantity associated with the effects of seismic waves radiated by the source fault [*Belardinelli et al.*, 1999] or as the static level that remains after the transient seismic waves have dissipated [*Okada* 1992; *Stein et al.*, 1992; *King et al.*, 1994]. Fault slip as a response to static-stress changes has been well documented for geometries similar to the Romanche and Prince Edwards events. For instance, the 1989 Loma Prieta earthquake on the San Andreas fault triggered slip on the subparallel Calaveras fault at points ~15-25 km from the Loma Prieta rupture zone [*McClellan*, 1990]. More recently, the 1998, M_w 8.2, strike-slip Antarctic event was calculated to have triggered off-fault aftershocks with focal mechanisms similar to the mainshock at distances over 80 km from the rupture zone [*Toda and Stein*, 2000]. It is not clear whether static or dynamic stresses are more relevant in triggering secondary ruptures that begin very soon after the passage of the S wave such as the Irpinia, Romanche, and Prince Edward Island events. However, the peak dynamic and static stress changes usually have the same sign and similar geometric patterns [*Belardinelli et al.*, 1999]. This should be particularly true for slow earthquakes where directivity effects are less likely to perturb the spatial pattern of the peak dynamic stresses. Therefore, we investigate whether the geometry of the Romanche and Prince Edward sequences, particularly the subevents located on the paleo-transforms, could have been consistent with the static stress changes produced by the initial slow components.

6.1. Stress Triggering Calculations for the 1994 Romanche Event

To calculate Δ_f on one fault as a result of slip on another, it is necessary to know the locations and focal mechanisms of both faults, the slip distribution on the source fault, and the effective friction coefficient on the receiver fault. For the 1994 Romanche event, the moment tensors of the slow component and the A and B subevents must be similar due to a lack of observable frequency dependence in the moment tensor [*McGuire et al.*, 1996]. The effective friction coefficient of the paleo-transform fault is unknown. We set μ =0.8, a value that provided a good fit to the aftershock distribution of the 1998 Antarctic earthquake which occurred in oceanic lithosphere [*Toda and Stein*, 2000]. The locations of the A and B subevents are constrained by high-frequency travel-time picks (Plate 1, [*McGuire et al.*, 1996]), but the location of the slow-precursor could not be determined owing to the poor signal to noise ratio at low-frequencies. One likely location for the slow-precursor is the seismic gap on the main transform between about -22.25° and -23.5° longitude. No events in the ISC catalog between 1964 and 1996 locate in this region (Plate 1A), indicating that the fault may have unusual rupture properties in this area. This location also shows unusual morphology in the transform valley with the active fault trace changing strike by ~18° near the location of a 1.5-km high ridge which interrupts the transform valley [*Searle et al.*, 1994]. Owing to the unusual nature of this region, we choose to test whether a slow precursor occurring in this area would have increased the likelihood of failure of parallel strike-slip faults at the locations of the 94A and 94B subevents.

To calculate Δ_f at the 94A and 94B subevent locations, we used a variety of uniform slip source-models that represent the uncertainty in the seismic moment, fault width, and stress drop for the slow precursor. The stress-drop uncertainty was parameterized in terms of α, the fault slip to length ratio, which ranges from about 10^{-4} to 10^{-5} [*Scholz et al.*, 1986]. Δ_f was calculated for each of the source models using a vertical right-lateral source fault, and assuming a vertical, right-lateral receiver faults. The calculations were done assuming a finite dislocation in an elastic half-space [*Okada* 1992; *Stein et al.*, 1992; *King et al.*, 1994]. The position of the source fault was then shifted along strike to find the location that maximized the sum of Δ_f at the 94A and 94B subevent locations, subject to the constraint that Δ_f be positive at both locations. The results (Table 6) indicate that a location for the slow precursor within the seismic gap can produce an increase in Δ_f at both subevent locations for each parameter combination. Plate 4A shows the results for parameter set 5 (Table 6). The spatial pattern of the predicted Δ_f values was similar for all cases tested. In particular, the lobe of positive Δ_f resulting primarily from an increase in shear stress along the strike of the fault overlapped the 94A location while the lobe of positive Δ_f resulting primarily from a decrease in normal-stress overlapped the 94B location. The values of Δ_f at the 94A location are generally smaller than those at the 94B location, but that difference would be lessened by a lower value of μ'.

The predicted values of Δ_f at the 94B location range from about .15 to .4 bars. This is in the range of Coulomb stress changes (.2-1.0 bars) which produced significant correlations with seismicity rate changes following several earthquakes including the 1992 Landers

Table 6. Coulomb Stress Changes Resulting from the 1994 Romanche Slow Precursor

Run	M_0	Depth (km)	α	L (km)	slip (m)	Shift (km)	Δ_f at A (bar)	Δ_f at B (bar)
1	0.7	0-5	.00001	65.13	.6513	-12	.027	.096
2	0.7	0-5	.00005	29.13	1.456	-22	.031	.179
3	0.7	0-5	.0001	20.60	2.059	-22	.030	.200
4	0.7	0-10	.00001	46.04	0.460	-17	.031	.140
5	0.7	0-10	.00005	20.60	1.030	-22	.033	.204
6	0.7	0-10	.0001	14.56	1.456	-22	0.33	.216
7	0.7	10-15	.00001	46.04	0.460	-32	.016	.086
8	0.7	10-15	.00005	20.60	1.030	-22	.033	.177
9	0.7	10-15	.0001	14.56	1.456	-22	.033	.186
10	1.4	0-5	.00001	92.11	.921	2	.039	.132
11	1.4	0-5	.00005	41.29	2.06	-17	.055	.302
12	1.4	0-5	.0001	29.13	2.912	-22	.062	.358
13	1.4	0-10	.00001	65.13	.6513	-12	.058	.193
14	1.4	0-10	.00005	29.13	1.45	-22	.068	.367
15	1.4	0-10	.0001	20.60	2.06	-22	.066	.409
16	1.4	10-15	.00001	65.13	.651	-12	.057	.166
17	1.4	10-15	.00005	29.13	1.45	-22	.067	.319
18	1.4	10-15	.0001	20.6	2.06	-22	.066	.354

where the M_0 values are x10^{19}Nm and the values of L and slip were calculated assuming a rigidity of 3.3x10^{10} Pa. The "Shift" denotes the distance it was necessary to shift the center point of the source fault in the x direction of Figure 9 to obtain the optimum alignment.

California, quake [*Stein et al.*, 1992] and the 1995 Kobe, Japan, earthquake [*Toda et al.*, 2000]. The magnitude of the Δ_f values is less important to this study than the spatial pattern. The uncertainties in subevent location, fault-zone rigidity, stress-drop, and slip distribution correspond to significant ($\geq$ a factor of 2) uncertainties in the Δ_f values. The calculation shown in Plate 4a is intended to show that the geometry of the static (and dynamic) stress changes is consistent with a slow-precursor in the seismic gap triggering the subevent on the offset paleo-transform. It is also interesting to note that a slow-precursor of similar size at the opposite, eastern end of the seismic gap would have increased Δ_f at the locations of both subevents of the 1971 sequence (Plate 4B). However, no low-frequency study has been done to evaluate whether such a precursor may have occurred in that earthquake.

6.2. Stress Triggering Calculations for the 1997 Prince Edwards Event

The 1997 Prince Edward Island event began with a ~30 s long smooth episode of moment-release that was nearly devoid of high-frequency energy (m_b 4.2) despite having a moment-magnitude of 6.2 [*McGuire and Jordan*, 2000]. This unusual event preceded an ordinary mainshock that ruptured a sub-parallel paleotransform offset from the main transform by about 40 km. Using the small amount of high-frequency energy radiated by the slow component and a temporary seismic network in southern Africa, we were able to locate the epicenter of the slow component (Plate 3). From the centroid location (Plate 3), we infer that the ruptures propagated to the south. Thus the fault orientation of the slow event is well constrained. However there is an uncertainty in the fault width and stress drop of the event. For large widths (10 km) and high stress-drops the mainshock is in a region of negative Δ_f (top panel, Plate 4C). However, for crustal scale widths (5 km) and low stress-drops, the location of the mainshock is near the boundary between positive and negative values of Δ_f (middle and bottom panels, Plate 4C). Owing to the uncertainties in event location and fault zone rigidity, the 97B subevent location could be in either a region of positive or negative Δ_f for the low stress drop case.

7. DISCUSSION

The 1994 Romanche and 1997 Discovery II earthquakes show remarkable similarities. Their P-waves begin with low-frequency ramps that indicate they initi-

ated with episodes of slow, smooth moment release that radiated little to no high-frequency energy. Both events occurred on transforms bounded by a transverse ridge and an adjacent paleo-transform boundary, and determination of their average directivity vectors indicates that more than one of these faults ruptured. While both the nature of the slow-precursor and the azimuth of the directivity are more tightly constrained for the 1997 event owing to higher data quality, the similarities between the two events are suggestive of a common type of slow source process that may occur regularly among large oceanic transform events.

While the primary traces of the Romanche and Discovery II transforms clearly are the plate boundaries for the majority of plate motion, it appears that the adjacent sub-parallel paleotransform faults may be accommodating a portion of the plate motion. We lack sufficient information about the slow components of the 1994 Romanche and Prince Edwards events to perform a more detailed calculation of the static and dynamic stress fields resulting from these events. However, it appears that in both cases, the faulting geometry could have been consistent with a triggering explanation. Triggering due to static stress changes has several unresolved issues with regard to these events. First, the complete lack of teleseismically recorded aftershocks for the 1994 Romanche event [*McGuire et al.*, 1996] indicates that triggering of seismicity by static stress changes may not be a commonly occurring phenomenon on these faults. Secondly, dynamic rather than static stress changes are more appealing to explain the close association in time of the slow and fast components of the Romanche and Prince Edwards sequences. Thus, the peak dynamic stresses, which show a similar spatial pattern to the static stress, may be more important in explaining the triggering of the off-fault subevents. While this model can only be shown to be consistent with the observed geometries, it does provide an explanation for the temporal proximity between the slow source process and the ordinary ruptures.

The apparent activity of the "paleotransform" faults has several interesting implications for both fault mechanics and tectonics problems. The paleotransforms adjacent to the Romanche and Discovery II transform faults appear to have been the primary plate boundaries until ~5-10 Ma and possibly even more recently. Thus the rate at which they strengthen and heal is related to the occurrence of the off-fault seismicity. After a transform fault passes a RTI, it appears to take approximately 2-4 Ma to completely heal as evidenced by seismicity (Plate 1D) and gravity studies of fracture zones [*Wessel and Haxby*, 1990]. Thus, it is not unreasonable that a fault could continue slipping for a few million years after it ceases to be the primary plate boundary. In fact, the stress perturbations resulting from large earthquakes on the main transform will systematically bring regions of the paleotransform closer to failure. Once a system of multiple sub-parallel faults is formed, the secondary fault(s) may be forced to remain active for a period of time until it completely heals, causing a distribution of plate-motion over a wider region than simply the primary transform valley. While the proposed activity of multiple faults is somewhat speculative, it clearly warrants further study using marine geologic, geodetic, and ocean bottom seismometer based methods.

Acknowledgments. We thank Ross Stein and Shinjie Toda for making their Coulomb stress change code available. All figures were generated using the GMT software freely distributed by *Wessel et al.* [1991]. This research was sponsored by the National Science Foundation under grant EAR-9805202. Woods Hole Oceanographic Institution contribution number J309.

REFERENCES

Abercrombie, R. E., and G. Ekström, Earthquake slip on oceanic transform faults, *Nature*, *410*, 74–77, 2001.

Backus, G. E., Interpreting the seismic glut moments of total degree two or less, *Geophys. J. R. astr. Soc.*, *51*, 1–25, 1977.

Belardinelli, M. E., M. Cocco, O. Coutant, and F. Cotton, Redistribution of dynamic stress during coseismic ruptures: Evidence for fault interaction and earthquake triggering, *J. Geophys. Res.*, *104*, 14,925–14,945, 1999.

Bohnenstiehl, D. R., M. Tolstoy, D. Smith, and C. G. Fox, Earthquake sequences detected using autonomous underwater hyudrophone data from the Northern Mid-Atlantic Ridge: February 1999-february 2000, *EOS, Trans. AGU*, p. F1077, 2000.

Bonatti, E., Subcontinental mantle exposed in the Atlantic Ocean on St. Peter-Paul islets, *Nature*, *345*, 800–802, 1990.

Bonatti, E., M. Ligi, L. Gasperini, A. Peyve, Y. Raznitsin, and Y. J. Chen, Transform migration and vertical tectonics at the Romanche fracture zone, equatorial Atlantic, *J. Geophys. Res.*, *84*, 21,779–21,802, 1994.

Bonatti, E., M. Ligi, A. M. Borsetti, L. Gasperini, A. Nergri, and R. Sartori, Lower Cretaceous depositis trapped near the equatorial Mid-Atlantic Ridge, *Nature*, *380*, 518–520, 1996.

Bonatti, E., L. Gasperini, M. Ligi, and A. N. B. Poliakov, Oceanic broad multi-fault transform plate boundaries, *Manuscript in preparation*, 2001.

Dziewonski, A. M., and D. L. Anderson, Preliminary reference Earth model, *Phys. Earth Planet. Inter.*, *25*, 297–356, 1981.

Dziewonski, A. M., G. Ekström, and N. N. Materovskaya, Centroid-moment tensor solutions for January-March 1998, in press,, *Phys. Earth Planet. Inter.*, 1999.

Ekström, G., J. Tromp, and E. W. Larson, Measurements and global models of surface wave propagation, *J. Geophys. Res.*, *102*, 8137–8157, 1997.

Forsyth, D. W., T. D. Bechtel, and L. M. Stewart, Rupture of separate en echelon segments of an oceanic transform fault in a single earthquake, *Eos. Trans. AGU.*, *67*, 359, 1986.

Gaherty, J. B., T. H. Jordan, and L. S. Gee, Seismic structure of the upper mantle in a central pacific corridor, *J. Geophys. Res.*, *101*, 22,291–22,309, 1996.

Gee, L. S., and T. H. Jordan, Generalized seismological data functionals, *Geophys. J. Int.*, *111*, 363–390, 1992.

Ihmlé, P. F., On the interpretation of subevents in teleseismic waveforms: The 1994 Bolivia deep earthquake revisited, *J. Geophys. Res.*, *103*, 17,919–17,932, 1998.

Ihmlé, P. F., and T. H. Jordan, Teleseismic search for slow precursors to large earthquakes, *Science*, *266*, 1547–1551, 1994.

James, D., et al., Southern Africa Seismic Experiment: Initial results, *Eos Trans. AGU*, *79* (17), Spring Meet. Suppl., S228, 1998.

Jordan, T. H., and K. A. Sverdrup, Teleseismic location techniques and their application to earthquake clusters in the south-central Pacific, *Bull. Seismol. Soc. Am.*, *71*, 1105–1130, 1981.

Kanamori, H., and G. S. Stewart, Mode of strain release along the Gibbs fracture zone, Mid-Atlantic Ridge, *Phys. Earth Planet. Inter.*, *11*, 312–332, 1976.

Kaverina, A. N., A. V. Lander, and A. G. Prozorov, Global creepex distribution and its relation to earthquake-source geometry and tectonic origin, *Geophys. J. Int.*, *125*, 249–265, 1996.

King, G. C. P., R. S. Stein, and J. Lin, Stress changes and triggering of earthquakes, *Bull. Seismol. Soc. Am.*, *84*, 935–953, 1994.

Klinger, Y., L. Rivera, H. Haessler, and J. Christopre Maurin, Active faulting in the Gulf of Aqaba: New knowledge from the m_w 7.3 earthquake of 22 November 1995, *Bull. Seismol. Soc. Am.*, *89*, 1025–1036, 1999.

McClellan, P. H., Triggered slip on the Calaveras fault during the magnitude 7.1 Loma Prieta, California, earthquake, *Geophys. Res. Lett.*, *17*, 1227–1230, 1990.

McGuire, J. J., and T. H. Jordan, Further evidence for the compound nature of slow earthquakes: The Prince Edward Island earthquake of April 28, 1997, *J. Geophys. Res.*, *105*, 7819–7828, 2000.

McGuire, J. J., P. F. Ihmlé, and T. H. Jordan, Time-domain observations of a slow precursor to the 1994 Romanche transform earthquake, *Science*, *274*, 82–85, 1996.

McGuire, J. J., L. Zhao, and T. H. Jordan, Measuring the second-degree moments of earthquake space-time distributions, *Geophys. J. Int.*, *145*, 661–678, 2001a.

McGuire, J. J., L. Zhao, and T. H. Jordan, Predominance of unilateral rupture for a global catalog of large earthquakes, *submitted to Bull. Seism. Soc. Am.*, 2001b.

Nostro, C., M. Cocco, and M. E. Belardinelli, Static stress changes in extensional regimes: An application to Southern Appennines (Italy), *Bull. Seismol. Soc. Am.*, *87*, 234–248, 1997.

Okada, Y., Internal deformation due to shear and tensile faults in a half-space, *Bull. Seismol. Soc. Am.*, *82*, 1018–1040, 1992.

Okal, E. A., and L. M. Stewart, Slow earthquakes along oceanic fracture zones: Evidence for asthenospheric flow away from hotspots?, *Earth Planet. Sci. Lett.*, *57*, 75–87, 1982.

Pinar, A., Source inversion of the 1993 and 1995 gulf of aqaba earthquakes, *Tectonophysics*, *283*, 279–288, 1997.

Scholz, C. H., C. Aviles, and S. G. Wesnousky, Scaling differences between large interplate and intraplate earthquakes, *Bull. Seismol. Soc. Am.*, *76*, 65–70, 1986.

Searle, R. C., M. V. Thomas, and E. J. W. Jones, Morphology and tectonics of the Romanche transform and its environs, *Mar. Geophys. Res.*, *16*, 427, 1994.

Silver, P. G., and T. H. Jordan, Total-moment spectra of fourteen large earthquakes, *J. Geophys. Res.*, *88*, 3273–3293, 1983.

Smith, D., M. Tolstoy, and C. G. Fox, Long term monitoring of seismicity at the Mid-Atlantic Ridge using autonomous underwater hydrophones, *EOS, Trans. AGU*, p. F1076, 2000.

Stein, R. S., G. C. P. King, and J. Lin, Change in failure stress on the southern San Andreas Fault system caused by the 1992 magnitude=7.4 Landers earthquake, *Science*, *258*, 1328–1332, 1992.

Stein, S., and A. Pelayo, Seismological constraints on stress in the oceanic lithosphere, *Phil. Trans. R. Soc. Lond.*, *337*, 53–72, 1991.

Su, W. J., R. L. Woodward, and A. M. Dziewonski, Degree 12 model of shear velocity heterogeneity in the mantle, *J. Geophys. Res.*, *99*, 6945–6980, 1994.

Toda, S., and R. Stein, Did stress triggering cause the large off-fault aftershocks of the 25 March 1998 Mw=8.1 Antarctic plate earthquake?, *Geophys. Res. Lett.*, *27*, 2301–2304, 2000.

Toda, S., R. Stein, P. A. Reasenberg, J. H. Dieterich, and A. Yoshida, Stress transferred by the 1995 M_w=6.9 Kobe, Japan shock: Effect on aftershocks and future earthquake probabilities, *J. Geophys. Res.*, *103*, 1998.

Wald, D. J., T. H. Heaton, and K. W. Hudnut, The slip history of the 1994 Northridge, California, earthquake determined from strong ground motion, teleseismic, GPS, and leveling data, *Bull. Seismol. Soc. Am.*, *86*, S49–S70, 1996.

Wessel, P., and W. F. Haxby, Thermal stresses, differential subsidence, and flexure at oceanic fracture zones, *J. Geophys. Res.*, *95*, 375–391, 1990.

Wessel, P., and W. H. F. Smith, Free software helps map and display data, *Eos Trans. AGU*, *72*, 441, 445–446, 1991.

Wiens, D. A., Effects of near source bathymetry on teleseismic p-waveforms, *Geophys. Res. Lett.*, *14*, 761–764, 1987.

Woodhouse, J. H., and A. M. Dziewonski, Mapping the upper mantle: Three-dimensional modeling of Earth structure by inversion of seismic waveforms, *J. Geophys. Res.*, *89*, 5953–5986, 1984.

Yoshida, S., Waveform inversion for rupture process using a non-flat seafloor model: application to the 1986 Andreanof Islands and 1985 Chile earthquakes, *Tectonophysics*, *211*, 45–59, 1992.

J. McGuire and J. Lian, MS 24 Woods Hole Oceanographic Institution, Woods Hole, MA, 02543

Tom Jordan, Department of Earth Sciences, Univ. of Southern California, Los Angeles, CA 90089-0740